Voltage Dip Induced Frequency Dips for Power Systems with High Shares of Wind Energy

Xianxian Zhao and Damian Flynn
School of Electrical and Electronic Engineering, University College Dublin
Belfield, Dublin 4, Republic of Ireland
xianxian.zhao@ucd.ie, damian.flynn@ucd.ie

***Abstract*—In order to limit drivetrain mechanical stress, wind turbine generators typically implement a delayed active power recovery following a voltage dip, which may result in a substantial reduction in system frequency, if many wind farms adopt a similar strategy, due to the resulting generation-demand imbalance. Therefore, based on a modified IEEE 39-bus system, the impact of active and reactive current priority strategies, and various reactive current loop controls for wind turbine generators on voltage dip induced frequency dips (VDIFDs) are examined. The effectiveness of local voltage control with reactive current priority is validated. In addition, if synchronous-based generation is displaced by grid-forming converters (GFMs), the frequency dips are less severe and the post-fault frequency recovers more quickly. However, due to reduced overcurrent capability, the GFM virtual angle control must be carefully designed to avoid transient instability, by, for example, reducing the droop gain. Finally, if DC-link voltage control and maximum power point tracking control for the grid-side and machine-side converters are switched (to simplify fault ride through implementation) care is needed to avoid large post-fault over-frequency transients for VDIFD events.**

Keywords—Voltage dip induced frequency dip, delayed active power recovery, grid-forming converter, wind turbine generator, fault ride through.

I. Introduction

To combat climate change, power systems around the world are rapidly transitioning from conventional fossil fuel- and synchronous machine-based generation to converter-based, variable wind and solar PV dominated renewable generation (a large fraction of which may be connected at distribution level), and high-voltage direct current (HVDC) transmission and interconnection with neighbouring systems [1]. In addition, power consumption is becoming more flexible, mainly due to gradual electrification of the transportation and heating sectors, and the integration of digital technologies and communication systems within power networks. In order to maintain secure and stable system operation, the stability of the resulting power system, and the capabilities of power electronic based generation are of specific interest, particularly under fault conditions [2][3].

In order to limit drivetrain mechanical stress, wind turbine generators typically implement a delayed active power output recovery after a severe fault. While conventional generators recover their active power output very quickly following a voltage dip, the slower (wind turbine) recovery can result in a substantial reduction in the system frequency, due to the generation-demand imbalance, particularly if a number of wind farms are located near to the fault location. The severity of the frequency dip depends on system inertia, active and reactive power regulation capability, and the reduction in wind power output during the fault, together with the wind power speed of recovery. In order to avoid cascade events, the rate of change of frequency (RoCoF), and the maximum frequency deviation, should be acceptably low, to avoid tripping loss of mains and/or under-frequency load scheduling protection relays.

EirGrid, the Irish transmission system operator, has identified voltage dip induced frequency dips (VDIFDs) as a future technical challenge [3], which has received limited attention in the literature [4]-[7]. Based on a modified IEEE 39-bus system, the impact on frequency nadirs, of different wind shares (up to 60%) and demand levels were studied in [4], with the post-fault active power recovery rates of wind turbine generators under different grid codes and load types studied in [5]. In [6], based on a future Ireland and Northern Ireland power system, studies were performed considering two retained wind power values and two post-fault recovery durations, with and without constant reactive current injection during faults, and with different reactive current rise times. In [7], focusing on PV power plants, active current recovery rates ranging from 10%/s to 1000%/s were studied, with a 100%/s rate providing the best behaviour in terms of voltage and frequency dynamics for a modified IEEE Nordic test system.

Distinct from existing works, this paper examines the impact of active and reactive current priority, reactive current loop control and the fault ride through strategy of wind turbine generators on VDIFD dynamics. The displacement of synchronous machines by grid-forming converters (GFMs) is also studied, considering their similar ability to create their own internal voltage angle and inherent inertial response, such that they can provide an immediate response to voltage and frequency disturbances [8][9]. GFMs can, however, offer faster and more flexible controllability than a synchronous machine, but their overcurrent capability is much less (typically 20% of rated current versus up to seven times for a synchronous machine [10]), and their control parameters must be carefully designed to ensure robustness.

Based upon high-fidelity electromagnetic transient (EMT) models of a modified IEEE 39-bus system (with modified WECC type 4B wind turbines by including phase-locked-loop (PLL) and inner current decoupling control) using Dymola software, the impacts of the delayed active power recovery of wind turbines on system dynamic stability are examined under bolted 3-phase faults in wind-rich regions. The main contributions of this paper are:

- The impact of the active and reactive current priority strategy, and different reactive current loop controls of wind turbine generators on voltage dip induced frequency dips are examined.
- The benefits of using local voltage control with reactive current priority for wind turbine generators to reduce voltage dip induced frequency dips is demonstrated.
- Post-fault frequency dynamic stability is compared when GFMs, or synchronous generators, represent the

dominant voltage sources. Different GFM control strategies are examined.

- The impact of the mechanical-side dynamics of a wind turbine generator on the fault ride through control implementation for VDIFDs is also examined.

The remainder of the paper is organized as follows: Section II describes the modified WECC wind turbine generator model, with droop control- and dispatchable virtual oscillator control (dVOC)-based GFMs. Section III presents the case studies and simulation results, and Section IV concludes the paper.

II. Modified WECC Wind Turbine Model with Droop Control and dVOC-based Grid-forming Converters

A. Modified WECC Wind Turbine Model

The modified WECC wind turbine type 4B model is shown in Fig. 1, with a phase-locked-loop (PLL), and active and reactive current decoupling control, incorporated to improve model correctness. The control details of *REEC_A* and *REGC_A* in the WECC wind turbine type 4B model are the same as Figures 3-1 and 3-2 in [11], and presented here as Figs. 2 and 3. The turbine representation, pitch angle control, and permanent magnet synchronous generator models follow [12]-[14]. To simplify the implementation of fault ride through control, the DC-link voltage is maintained by the machine-side converter (MSC), while maximum power point tracking (MPPT) is achieved by the grid-side converter (GSC) [15].

B. Droop Control-based Grid-Forming Converter

A voltage source converter with a LCL filter, operating under droop-based grid-forming control is shown in Fig. 4. The droop grid-forming control includes outer P/f and Q/V droop control loops, inner cascaded voltage and current control loops, damping enhancement, and threshold virtual impedance current limiting control. The controlled current source on the DC side is intended to represent the energy source dynamics. The structure of the virtual impedance control follows that of [16][17], while the virtual impedance parameters are tuned such that the converter current is limited within 1.2 pu (ignoring initial transient) when a bolted 250 ms, 3-phase fault is applied at the point of common coupling. The voltage and current PI controller parameters follow [16], which are designed to provide optimal damping for a GF connected to a grid with a high short-circuit ratio. It is noted that virtual synchronous generator grid-forming control, i.e. swing equation replaces P/f droop loop in Fig. 4, is not directly studied here, since it is equivalent to Fig. 4 under constant P^*.

C. Dispatchable Virtual Oscillator (dVOC) Control-based Grid-Forming Converter

The dispatchable virtual oscillator control shown in Fig. 5, as proposed in [18], adopts a different approach for generating the voltage amplitude and angle references, by considering the respective couplings between reactive and active power. In order to ensure that the dVOC GF active and reactive power droop settings are equivalent to a droop-based GF for the study in Section III, the following definitions are made: $\eta = m_p$, $\alpha = m_q$.

III. Case Studies and Simulation Results

A modified version of the New England 39-bus system [19], Fig. 6, with the synchronous generators at buses 32, 33, and 35 replaced by wind farms (WFs), resulting in a 46% wind energy share, is used to study voltage dip induced frequency dips. The synchronous machines are equipped with automatic voltage regulators, power system stabilizers, and turbine governors, Fig. 7. The inertial constant of the synchronous machine at bus 39 is reduced from 50 to 5 s to represent a more standalone grid. Constant impedance loads and equivalent π electrical lines are modelled. The total active and reactive power output of the generators of 6.14 GW and 1.25 GVAr are unchanged. Each WF is represented by an aggregated wind turbine model, Fig. 1. The active current recovery rate in REGC_A block, *rrpwr*, is set to 35%/s, which lies between a limit of 20%/s, as defined by the German grid code [20], and of 100%/s, as defined in Great Britain for faults with a duration greater than 140 ms [21], while the reactive current recovery rate is not limited. Wind turbine and GF converter parameters are listed in Tables I-II. Simulations are performed within the Dymola environment (0.1 ms step size).

A. Impact of active/reactive current priority, and reactive current control on voltage dip induced frequency dips

Case 1: With a bolted 140 ms, 3-phase fault applied at bus 16, being one of the weaker buses in the network.

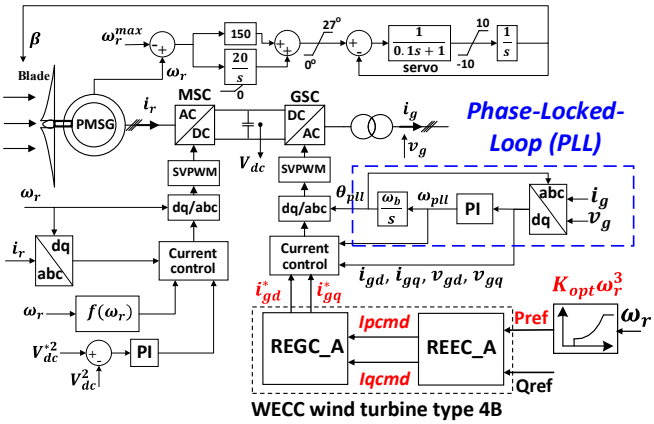

Fig. 1. Modified WECC wind turbine type 4B model by including PLL, inner current decoupling control, with MPPT and DC-link voltage control converter roles switched.

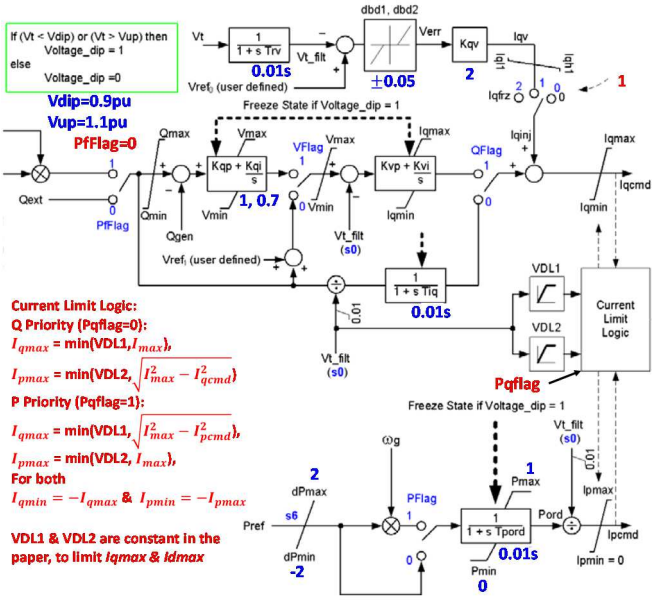

Fig. 2. REEC_A block details in the WECC wind turbine type 4B model.

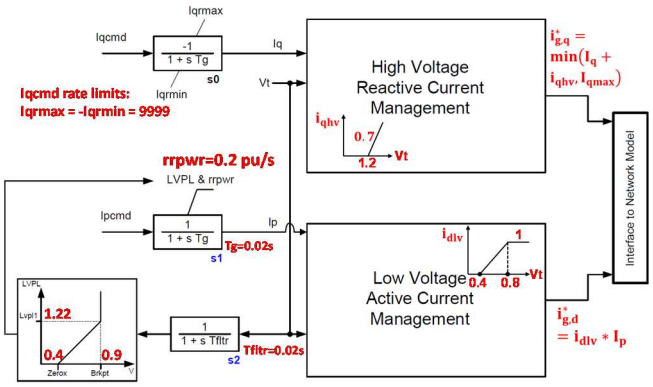

Fig. 3. REGC_A block details in the WECC wind turbine type 4B model.

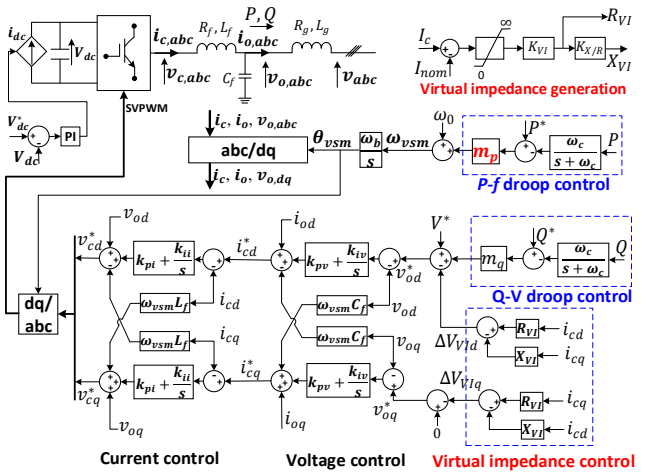

Fig. 4. Droop control-based grid-forming converter.

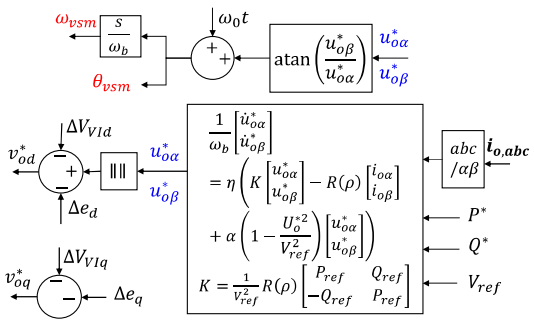

Fig. 5. Dispatchable virtual oscillator control (dVOC)-based GFM, with remainder of model the same as Fig. 2.

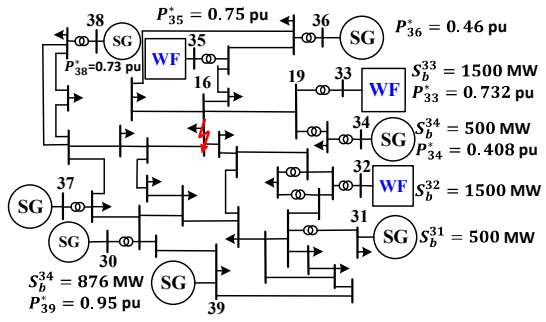

Fig. 6. Modified 39-bus system with the synchronous generators at buses 32, 34 and 35 replaced by grid-following control based wind farms.

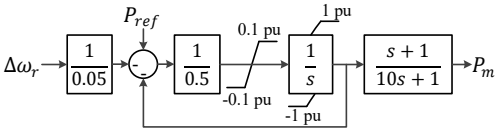

Fig. 7. Turbine governor control for the synchronous machines.

Six scenarios are considered with the WFs operating under constant reactive power, local voltage or local coordinated Q/V control, and either active or reactive current prioritized. Comparison is then made against an additional scenario with the WFs replaced by synchronous machines with the same MVA rating, and power and voltage setpoints. In Case 1, the mechanical side dynamics are not studied, such that the "upstream" GSC dynamics of a wind turbine generator, Fig. 1, are represented by a constant DC voltage source, with P_{ref} for the GSC assumed constant. The converter current limit, I_{max}, is 1.1 pu, the same as I_{qmax} or I_{pmax} (depending on implemented current priority). The gains for the local voltage PI controller are selected as 2 and 1.4.

Results for Case 1 are shown in Figs. 8 and 9. Fig. 8(a) shows that the post-fault (centroid) frequency, based on the MVA weighted average of the SG rotor speeds, for the synchronous machine based system quickly recovers to the pre-fault value. However, when the 3 WFs are introduced, it requires a few seconds for the wind farms to return to full output (*rrpwr* = 35 %/s), as seen in Fig. 8(b), resulting in large frequency dips after clearing the fault, such that it takes ≈20 s for steady-state conditions to be achieved.

Fig. 8(a)(b) shows that with active current priority, irrespective of the reactive current control implemented, that the post-fault active power of the WFs is lower, and hence the frequency dips are deeper than for reactive current priority. It is helpful here to consider the WF at bus 33 under active or reactive current priority with constant reactive power control (i.e. red and blue lines), Fig. 9. Under active current priority, during the fault, the active current reference I_{pcmd} from the outer REEC_A block reaches its current limit of 1.1 pu, and the reactive references I_{qcmd} and i^*_{gq} reduce to zero (as seen in Fig. 9(b)). Subsequently, the terminal voltage, V_t, (Fig. 9(a)), is also low, which leads to I_p in the REGC_A block being very low, due to low voltage power limiter logic (LVPL), although I_{pcmd} is high (Fig. 9(c)). After the fault is cleared, I_p recovers, but with the ramp rate limited by *rrpwr*, the active power output is low, and the frequency dip large (≈1.4 Hz), as seen in Fig. 8(b)(a) (If a smaller *rrpwr* is used the frequency nadir is lower, which is not shown here due to the space limitation). Fig. 9 shows that under reactive current priority, during the fault, I_{qcmd} is high, which results in V_t being higher than under active current priority, and hence I_p is non-zero (non-zero I_p is also due to non-zero I_{pcmd}). Hence, after the fault is cleared, I_p (and i^*_{gd}) recovers from a higher starting point, so that pre-fault conditions are achieved more quickly.

Under the same reactive current priority, Fig. 8(a) shows that the post-fault frequency dip under local voltage control is larger than under constant reactive power control, although the terminal voltage V_t is higher in the former scenario, Fig. 9(a). Under local voltage control, I_{qcmd} reaches I_{max} (1.1 pu), leading to I_{pcmd} and I_p being zero during the fault. Thus, the post-fault active power recovery is lower and the frequency dip deeper, as seen in Figs. 8 and 9. With I_{pcmd} being zero during the fault, it follows that the frequency dip transients look similar, Fig. 8(a), under different reactive current loop controls with active current priority. Fig. 8(a) also shows that the frequency dip with coordinated Q/V control lies between the extremes of constant reactive power and voltage control.

In conclusion, in order to lessen the impact of voltage dip induced frequency dips, irrespective of the assigned current priority and reactive current loop control, during the fault, I_{pcmd} should be non-zero, but, V_t should not be too low,

causing I_p to be too low (V_t limits I_p through LVPL logic). Based on this principle, for a wind turbine generator during a fault, the reactive current support should be sufficiently high to support the terminal voltage, while, at the same time, converter current capacity should also be assigned to the active current, such that $I_{dmax} \neq 0$.

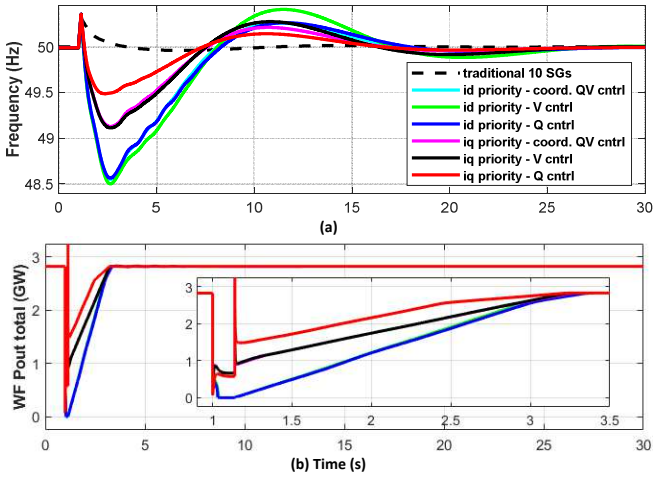

Fig. 8. System (centroid) frequency and total active WF power for Case 1.

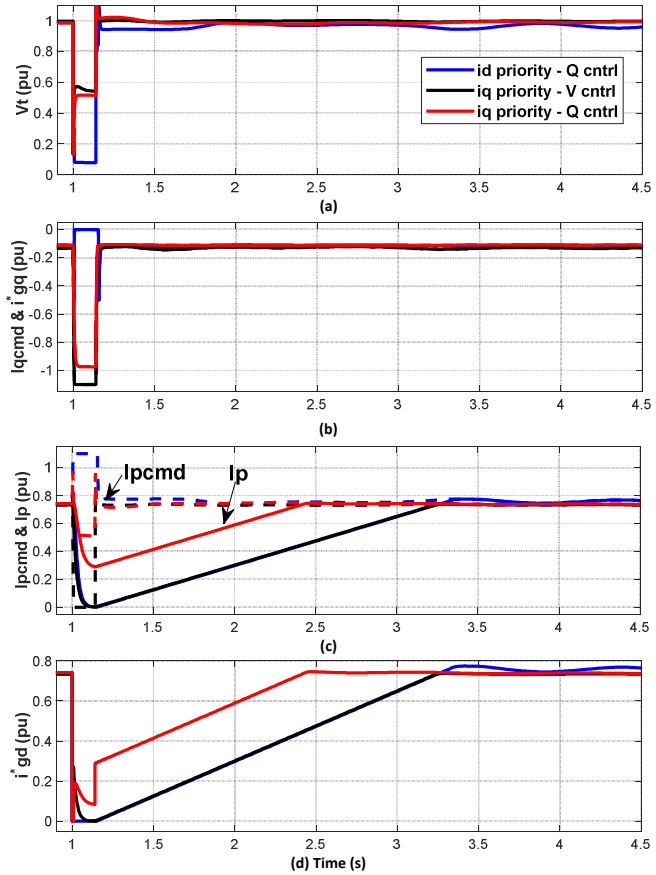

Fig. 9. Terminal voltage, active power output and d- and q-axis current signals of REEC_A and REGC_A block of the WF at bus 33 for Case 1.

B. Reactive current priority and local voltage control with I_{qmax} as large as possible and $I_{qmax} < I_{max}$

Case 2: The benefits of using reactive current priority and local voltage control, with I_{qmax} made as large as possible and $I_{qmax} < I_{max}$, to improve voltage dip induced frequency performance are now investigated. The settings of Case 2 are the same as Case 1, but now I_{max} is increased from 1.1 pu to 1.2 pu, and 1.3 pu, while I_{qmax} is limited to 1.1 pu, or 1.2 pu. The WFs are operated under reactive current priority and local voltage control, with the PI gains doubled from those in Case 1 (to increase the reactive power reference towards I_{qmax} during the fault).

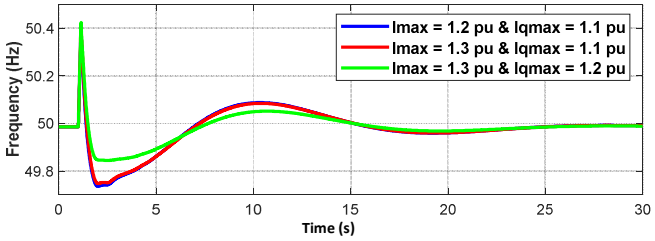

Fig. 10. System (centroid) frequency for Case 2.

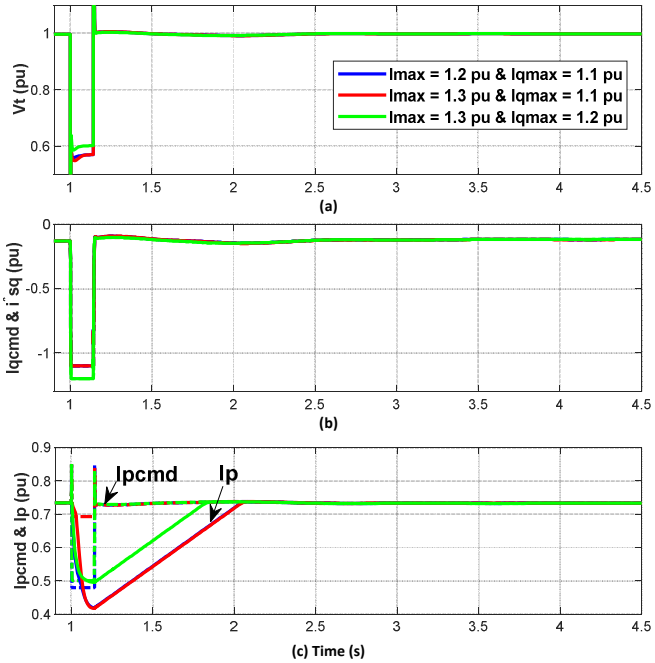

Fig. 11. Terminal voltage, and d- and q-axis current signals of REEC_A and REGC_A block of the WF at bus 33 for Case 2.

Results for Case 2 are shown in Figs. 10 and 11 for the same fault conditions at the same bus as Case 1. Comparing equivalent *i_q priority – V cntrl* strategies, and I_{qmax} = 1.1 pu, between Figs. 9 and 11 shows that the terminal voltage, V_t, during the fault is almost the same, since I_{qcmd} reaches its maximum value (1.1 pu). However, the frequency dip in Fig. 10 is much reduced over that in Fig. 8(a) (solid black line), since $I_{qmax} < I_{max}$ in Case 2 replaces $I_{qmax} = I_{max}$ in Case 1, leading to I_{pcmd} increasing from zero to a non-zero value. Hence, for the same V_t, I_p is increased, and the post-fault active power output is higher. Fig. 10 also indicates that the frequency dip under *i_q priority – V cntrl* and I_{qmax} = 1.1 pu in Case 2 is reduced, as compared to *i_q priority – Q cntrl* and I_{qmax} = 1.1 pu (red line) in Case 1. This is because during the fault, for Case 2, I_{qcmd} reaches 1.1 pu under local voltage control, while for Case 1, I_{qcmd} is only 0.98 pu. Hence, V_t is higher during the fault for Case 2, leading to a larger I_p (0.42 pu compared to 0.3 pu in Case 1), and an improved post-fault active power recovery, as seen when comparing results in Figs. 9 and 11. The effectiveness of the proposed reactive current priority strategy, together with local voltage control (with $I_{qmax} < I_{max}$) is, therefore, verified. Note that during faults, local voltage control always ensures positive reactive current support, while constant reactive power control with $Q_{ref} < 0$ will result in negative reactive current support.

Fig. 10 shows that the frequency response shapes are very similar when I_{qmax} = 1.1 pu, despite different I_{max} limits, given that, during the fault, I_{qcmd} are the same, and hence V_t are the same, leading to the same I_p, although I_{pcmd} is larger when I_{max} = 1.3 pu. Similarly, the frequency dip when I_{qmax} = 1.2 pu and I_{max} = 1.3 pu is smaller than when I_{qmax} = 1.1 pu and I_{max} = 1.3 pu, since increasing I_{qmax} enables I_{qcmd} to be higher, from which it follows that V_t is higher, I_p is higher, with the end result that the post-fault active power recovery is improved, as seen in Fig. 11. As anticipated, it can be concluded that I_{qmax} should be made as large as possible.

C. Post-fault frequency dynamic stability with SGs replaced by different grid-forming converters

Case 3: The scenario *i_d priority – Q cntrl* in Case 1 is now re-examined, but the full WF model, Fig. 1, is used to assess the impact of the mechanical-side dynamics (with the MPPT and DC-link voltage control converter roles switched for the fault ride through control implementation) on post-fault frequency stability. Four further scenarios are defined: (1) all synchronous generators are replaced by droop-based GFMs, with a droop coefficient, m_p, of 0.02; (2) replaced by dVOC GFMs with η (= m_p) of 0.02; replaced by (3) droop-based or (4) dVOC GFMs with a smaller droop coefficient of 0.005. The droop-based and dVOC GFMs assume the same MVA rating, voltage and active/reactive power setpoints as the synchronous generators. Note that the GFMs, Figs. 4 and 5, with m_p being higher than 0.02 indicate a low stability margin for fault events.

The simulation results for Case 3 are shown in Figs. 12 - 14. As seen in Fig. 12(a), when the synchronous machines are replaced by GFMs, irrespective of the grid-forming control strategy, the voltage dip induced frequency dips are greatly improved, and the system frequency recovers quickly with limited oscillation. In addition, the total active and reactive power output responses of the WFs in Fig. 12(b)(c) are very similar, irrespective of whether synchronous machines or GFMs are in place, demonstrating that the GFs offer faster active/reactive power regulation capability compared to their synchronous machine equivalents. However, for the *Droop – i_d priority* and *dVOC – i_d priority* (m_p = 0.02) scenarios, frequency oscillations are seen in Fig. 12(a), due to the GFM at bus 39 becoming unstable after the fault is cleared (The GFM at bus 39 is affected more than others, since its initial active power output is already high at 0.95 pu). Fig. 13(a)(b) reveals that the GFM virtual angular speed at bus 39 experiences a large overshoot and the active power output falls negative (before regaining stability). Fig. 13(c) also shows that the GFM current exceeds the current limit of 1.2 pu under threshold virtual impedance current limiting control. When m_p is reduced from 0.02 to 0.005, Fig. 12(a), the previous oscillations disappear, since the GFM at bus 39 now remains stable, as a result of the increase in the virtual angle for the GFM during the fault being reduced, Fig. 13(a).

The stability of the grid-forming converters with m_p set at 0.005 is seen in Fig. 13(b)(c), since the active power output during the post-fault period is (temporarily) above the pre-fault value, with the current limited within 1.2 pu. It follows that although GFMs can offer much faster controllability than synchronous machines, their limited overcurrent capability means that the virtual angle control should be carefully designed to avoid transient instability during a fault, by, for example, reducing the droop coefficient, as demonstrated here, or freezing the virtual angular speed [9]. Amongst various factors, the pre-fault active power output, GFM current limit and transmission line strength should be considered as part of the design process.

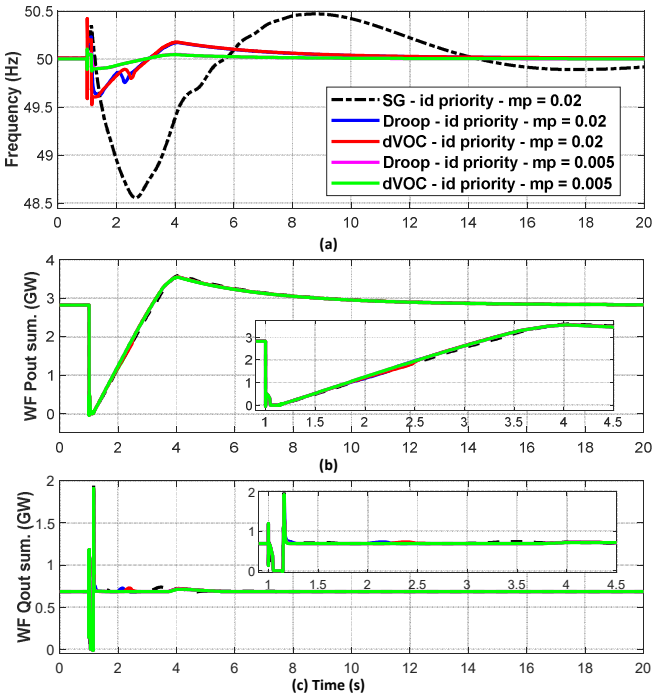

Fig. 12. System (centroid) frequency, and total active and reactive power output of the WFs for Case 3.

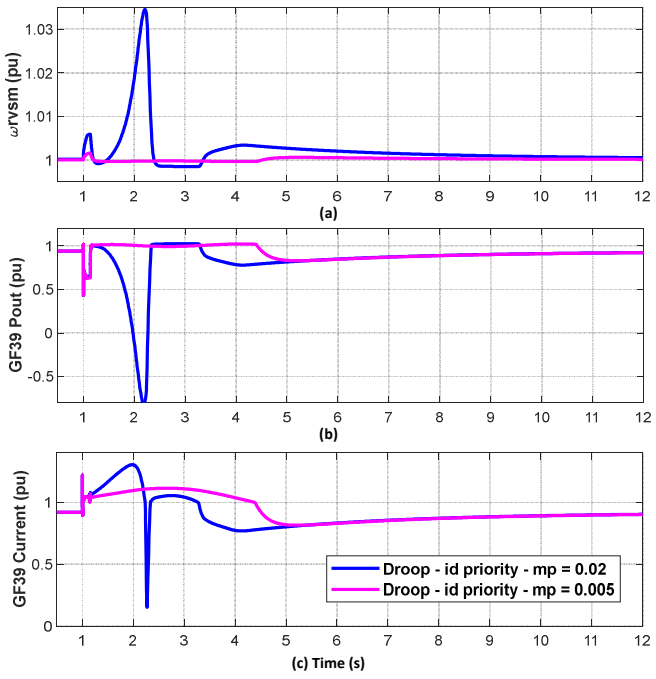

Fig. 13. Virtual angular speed, active power output and converter current of droop-based GFM at bus 39 with m_p selected as 0.02 or 0.005 for Case 3.

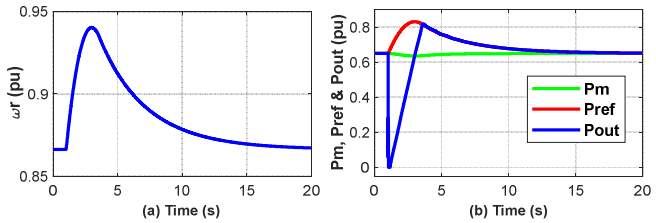

Fig. 14. Rotor speed, aerodynamic input power, active power reference, and output power of WF at bus 32 for Case 3 under *SG – i_d priority* scenario.

Finally, under i_d priority, comparing the blue trace in Case 1, Fig. 8(a), where a constant P_{ref} is given, against the black dashed trace in Case 3, Fig. 12(a), indicates that when the WFs are supplied with a MPPT control reference, $P_{ref} = K_{opt}\omega_r^3$, that the frequency nadir is largely unchanged, but the over-frequency is much larger. For the same event, Fig. 14, rotor speed, and hence $P_{ref} = K_{opt}\omega_r^3$ increase during the period 30–33 s, due to delayed active power recovery of the WF (input aerodynamic wind power almost unchanged, green line). It can subsequently be concluded that switching the MPPT and DC-link voltage control roles (to simplify fault ride through implementation), can lead to over-frequency concerns for voltage dip induced frequency dip events.

TABLE I. DROOP AND DVOC-BASED GRID-FORMING CONVERTER

Parameter	**Value (pu)**	**Parameter**	**Value (pu)**
R_f , L_f , C_f	0.005, 0.15, 0.066	k_{pv} , k_{iv} , k_{pi} , k_{ii}	0.52, 1.161022, 0.7388, 1.19
R_g , L_g	0.005, 0.15	I_{nom} , R_{VI} , X_{VI}	1, 0.67, 5
For droop GFM		For dVOC GFM	
m_p , m_q , m_c	0.02, 0.0001, 31.4 rad/s	η , α , ρ	m_p , $1/m_q$, 30

TABLE II. PMSG AND CONVERTER CONTROL PARAMETERS

Parameter	**Value (pu)**	**Parameter**	**Value (pu)**
Permanent magnet synchronous generator (PMSG)			
Rated machine power / current	2 MVA / 0.29 kA	Machine poles / PM flux	22 / 1.3 pu
Machine d-/q-axis magnetising inductance	1 pu/ 0.65 pu	Stator resistance / Leakage inductance	0.01 pu / 0.1 pu
Generator + turbine inertia constant	5.05 s	MSC & GSC rated power	2 MVA / 2.5 MVA
MSC & GSC rated voltage	4 kV	DC Bus C_{dc}	311 µF
Machine-side converter (MSC) control			
V_{dc} PI gains	6.8, 74.5	Current PI gains	200, 5000
Grid-side converter (GSC) current control			
Current PI gains	70, 171	PLL PI gains	6, 10

IV. CONCLUSIONS

Voltage dip induced frequency dips due to delayed active power recovery from wind farms under severe faults have been investigated on a modified IEEE 39-bus power system. Simulation results show that the delayed active power recovery can lead to a more severe frequency nadir when priority is given to the wind turbine generator active current during a fault, since the lower terminal voltage affects the active current reference, due to introducing low voltage protection against drivetrain mechanical stress. However, when adopting the proposed reactive current priority, and local voltage control with I_{qmax} made as large as possible, and $I_{qmax} < I_{max}$, the impact of frequency dips, following on from fault events, is greatly reduced. It is also seen that the frequency nadirs are improved and that the frequency recovers faster when the synchronous machines are displaced by droop or dVOC based GFMs. However, due to their lower overcurrent capability, the control approach for the GFM virtual angle should be carefully designed to avoid transient instability, by, either reducing the droop coefficient, as demonstrated in this paper, or freezing the virtual angular speed [9]. Switching the converter roles of a wind turbine generator, for MPPT and DC-link voltage control, to simplify fault ride through implementation, also requires careful consideration to avoid over-frequency transients during the post-fault period.

ACKNOWLEDGMENT

Xianxian Zhao is supported by Science Foundation Ireland under Investigator Award SFI/15/IA/3058.

REFERENCES

[1] B.M.S. Hodge, et al., "Addressing technical challenges in 100% variable inverter - based renewable energy power systems," *Wiley Interdiscipl. Rev.: Energy and Environ.,* vol. 9, no. 5, p. e376, 2020.

[2] EirGrid and SONI, "Shaping our electricity future – a roadmap to achieve our renewable ambition," Nov. 2021, Available: https://www.eirgridgroup.com/site-files/library/EirGrid/Shaping_Our_Electricity_Future_Roadmap.pdf.

[3] EirGrid and SONI, "Potential solutions for mitigating technical challenges arising from high RES-E penetration on the Island of Ireland - a technical assessment of 2030 study outcomes," 22 Dec. 2021, Available: http://test.soni.ltd.uk/media/documents/Technical-Assessment-of-2030-Study-Outcomes.pdf.

[4] Z.H. Rather and D. Flynn, "Impact of voltage dip induced delayed active power recovery on wind integrated power systems," *Control Eng. Pract.*, vol. 61, pp. 124-133, 2017.

[5] H. Karbouj and Z.H. Rather, "A comparative study on the impact of grid code regulations on stability of wind integrated power systems," in *Proc. 2019 IEEE 1st Glob. Power, Energy and Commun. Conf.*, Nevsehir, Turkey, 2019.

[6] H.W. Qazi, et al., "Impacts of fault ride through behavior of wind farms on a low inertia system," *IEEE Trans. Power Syst.*, DOI: 10.1109/TPWRS.2020.3003470, 2020.

[7] G. Lammert, et al., "Control of photovoltaic systems for enhanced short-term voltage stability and recovery," *IEEE Trans. Energy Convers.*, vol. 34, no. 1, pp. 243-254, 2018.

[8] X. Zhao, P. G. Thakurta, and D. Flynn, "Grid-forming requirements based on stability assessment for 100% converter - based Irish power system," *IET Renew. Power Gener.,* vol. 16, no. 3, pp. 447-458, 2022.

[9] X. Zhao and D. Flynn, "Stability enhancement strategies for a 100% grid - forming and grid - following converter - based Irish power system," *IET Renew. Power Gener.,* vol. 16, no. 1, pp. 125-138, 2022.

[10] G. Denis, et al., "The Migrate project: the challenges of operating a transmission grid with only inverter-based generation. A grid-forming control improvement with transient current-limiting control," *IET Renew. Power Gener.*, vol. 12, no. 5, pp. 523-529, 2018.

[11] P. Pourbeik, "WECC Second Generation Wind Turbine Models: Specification of the Second Generation Generic Models for Wind Turbine Generators", [online] Available: https://www.wecc.biz/Reliability/WECC%20Second%20Generation%20Wind%20Turbine%20Models%20012314.pdf.

[12] N. P. Strachan and D. Jovcic, "Stability of a variable-speed permanent magnet wind generator with weak AC grids," *IEEE Trans. Power Del.*, vol. 25, no. 4, pp. 2779-2788, 2010.

[13] J.G. Slootweg, et al., "General model for representing variable speed wind turbines in power system dynamics simulations," *IEEE Trans. Power Syst.*, vol. 8, no. 1, pp. 144–151, Feb. 2003.

[14] J. de Almeida and R.G. Lopes, "Participation of doubly fed induction wind generators in system frequency regulation," *IEEE Trans. Power Syst.*, vol. 22, no. 3, pp. 944–950, Aug. 2007.

[15] H. Geng, et al., "Unified power control for PMSG-based WECS operating under different grid conditions," *IEEE Trans. Energy Convers.,* vol. 26, no. 3, pp. 822-830, 2011.

[16] T. Qoria, et al., "Local control and simulation tools for large transmission systems," EU H2020 MIGRATE WP3, 2019. Available: https://www.h2020-migrate.eu/downloads.html. [Accessed: 26/3/20]

[17] A.D. Paquette and D.M. Divan, "Virtual impedance current limiting for inverters in microgrids with synchronous generators," *IEEE Trans. Ind. Appl.*, vol. 51, no. 2, pp. 1630-1638, 2014.

[18] D. Groß, et al., 'The effect of transmission-line dynamics on grid-forming dispatchable virtual oscillator control', *IEEE Trans. Contr. Netw. Syst.*, 2019, 6, (3), pp. 1148-1160.

[19] I. Hiskens, "A study of an IEEE 10-generator, 39-bus system," IEEE PES Task Force Benchmark Syst. Stability Controls, Tech. Rep., Nov. 2013. [Online]. Available: http://www.sel.eesc.usp.br/ieee/.

[20] VDE-AR-N 4120, "Technical requirements for the connection and operation of customer installations to the high-voltage network (TCC High-Voltage)," Jan. 2015.

[21] National Grid, "Guidance Notes – Power Park Modules," Is. 3, 2012.